Taylor & Francis
Taylor & Francis Group

Check for updates

HVSR-based Site Classification Approach Using General Regression Neural Network (GRNN): Case Study for China Strong Motion Stations

Kun Ji [a], Yefei Ren[a], Ruizhi Wen[a], ChuanBin Zhu[b], Ye Liu[a], and Baofeng Zhou[a]

[a]Key Laboratory of Earthquake Engineering and Engineering Vibration Institute of Engineering Mechanics, China Earthquake Administration, Harbin, China; [b]GFZ German Research Centre for Geosciences, Helmholtz Centre Potsdam, Potsdam, Germany

ABSTRACT

Seismic site classification, which is fundamental for site-specific seismic hazard assessment, also plays an important role in accurate interpretation of ground motion data. However, detailed borehole information is not always available in many countries, e.g., China. Therefore, this study investigated application of the generalized regression neural network (GRNN) method to seismic site classification using China strong motion stations as example case. First, stations from KiK-net in Japan were classified based on their borehole information and individually assigned to I, II, III, and IV site classes as defined in Chinese seismic code. Then, mean horizontal-to-vertical spectral ratio (HVSR) curves for each site class were calculated as reference patterns. The overall recall rates for I, II, and III sites could reach 66.60%, 67.57%, and 68.42%, respectively, regarding use of KiK-net stations. The GRNN site classification scheme was validated using borehole information of K-NET stations, with recall rates for I and II site classes reaching 68% and 60%, respectively. Finally, based on HVSR curves calculated using strong ground motion data acquired during 2007–2015 in China, the site conditions of 167 National Strong Motion Observation Network System stations were estimated using the GRNN classification scheme. The results were partially validated using borehole information of 73 stations. The similarity between the mean HVSR curves and reference pattern curves indicated that the GRNN seismic site classification scheme is robust and could produce plausible results succinctly.

1. Introduction

Many post-earthquake investigations have proven that local site effects can have considerable influence on ground motion features and structural dynamic response (e.g., Seed et al. 1988; Tsai and Huang 2000; Wood 1908). In many countries, it has been common practice to incorporate site classification work in seismic code provisions. The most commonly applied site classification index is the average shear wave velocity in the upper 30 m (V_{S30}), as recommended by the National Earthquake Hazards Reduction Program (NEHRP) (BSSC, 2003). Moreover, proper use of large numbers of ground motion data requires that local site conditions of recording be considered comprehensively, e.g., when used in state-of-the-art Next-Generation Attenuation (NGA) ground motion models. However, owing to the limited availability of drilling borehole data in many countries, e.g., China, application of the V_{S30} is not always practicable for site classification of strong ground motion stations.

CONTACT Yefei Ren renyefei@iem.net.cn Key Laboratory of Earthquake Engineering and Engineering Vibration Institute of Engineering Mechanics, China Earthquake Administration, Harbin, China

Considering the potential financial or technical constraints in obtaining borehole information, various researchers have sought to determine site class using ground motion data. One approach popular for evaluating site conditions is the horizontal-to-vertical spectral ratio (HVSR) method using either earthquake recordings or ambient seismic noise. The HVSR method can be used to estimate site horizontal amplification at different periods supposing that vertical component amplification is negligible. The HVSR method does not require a proper rock reference station, which is an advantage that has led to its widespread use in site classification of strong ground motion observation networks over the world, e.g., Japan, Italy, Iran, and China (Alessandro et al. 2012; Fukushima et al. 2007; Ghasemi et al. 2009; Wen et al. 2014; Zhao et al. 2006).

Although the basic concept of HVSR is rational, it is not easy in practice to accurately classify site conditions by relying solely on the predominant period of HVSR curves. Some automatic empirical schemes have been proposed to settle this issue. For example, Zhao et al. (2006) suggested use of the probabilistic distribution difference of H/V spectral ratios of all periods to measure the similarity between a reference curve and the HVSR curves to be classified. For a more effective evaluation of the degree of similarity of the HVSR shape, Ghasemi et al. (2009) constructed an empirical identification index using Spearman's correlation coefficients. For Chinese seismic code defined site classes, a satisfactory success rate could not be simultaneously achieved for each site class using these two empirical methods, according to validation results based on borehole information of KiK-net stations (Ji, Ren, and Wen 2017). In addition to the varied and complex characteristics of the seismic site response, the relatively wide ranges of shear wave velocity and sediment thickness for the II site class are the main obstacles in relation to Chinese seismic site classification. In previous work, we proposed an empirical site classification scheme that considers many factors that include the amplitude, predominant period, and shape similarity of HVSR curves (Ji, Ren, and Wen 2017). Using this scheme, the success rates for KiK-net stations in identifying I, II, and III site classes could reach 63%, 64%, and 58%, respectively. However, the empirical classification scheme is complex and requires subjective predefinition of both the boundary of the predominant period and the threshold of the amplitude for the I site class, which relies largely on user experience and judgment.

Yaghmaei-Sabegh and Tsang (2011) proposed the use of artificial neural networks (ANNs) for seismic site classification with predefined reference HVSR curves regarding different site classes. Using this scheme, sites are classified into four types based on the mean reference HVSR curves obtained from Iran (Ghasemi et al. 2009) and Japan (Zhao et al. 2006). The proposed approach has been validated using data of the 1999 Chi-Chi earthquakes and the 2017 Mw 7.3 Ezgeleh earthquake in Iran (Yaghmaei-Sabegh and Rupakhety 2020; Yaghmaei-Sabegh and Tsang 2011). By assigning weights to the results of ANN-based site classification scheme and empirical site classification methods (Phung, Atkinson, and Lau 2006; Zhao et al. 2006), Yaghmaei-Sabegh and Tsang (2014) estimated the site condition of the East-Azerbaijan Province in the northwestern part of Iran. All these studies focused on seismic site classification based on recordings from a specific earthquake event or regional seismographic network with dense recordings. In this study, we will further develop this approach and apply it to national strong ground motion stations in China.

We first established reference patterns using KiK-net stations' HVSR curves. Then the results were validated using borehole information of K-NET stations. After that, the generalized regression neural network (GRNN) scheme was applied to China's National Strong Motion Observation Network System (NSMONS) stations using ground motion recordings during 2007–2015.

2. Empirical Reference HVSR Curves

2.1. Site Class Definition in Chinese Seismic Code

Unlike the definitions in the NEHRP, there are four site classes in Chinese seismic code (MHURC, 2010), which are determined according to two indices: the equivalent shear wave velocity of the sediment (V_{se}) and the thickness of the soil layer (H^*). The boundaries for these two parameters are

Table 1. Definition of site classes in Chinese seismic code (GB50011-2010) (Ministry of Housing and Urban-Rural Construction of the People's Republic of China (MHURC) 2010).

Equivalent shear wave velocity $V_{se}/(m \cdot s^{-1})$	Thickness of soil layer, H^*/m				
	I_0	I	II	III	IV
>800	0				
$500 < V_{se} \leq 800$		0			
$250 < V_{se} \leq 500$		<5	≥5		
$150 < V_{se} \leq 250$		<3	$3 \leq H^* \leq 50$	>50	
≤150		<3	$3 \leq H^* \leq 15$	$15 < H^* \leq 80$	>80

presented in Table 1. The site class was defined according to these two indices both. It should be noted that I_0 is a subclass of site class I. Generally, H^* is defined as the depth above the engineering bedrock layer where $V_s \geq 500$ m/s. If there exists a soil layer with a value of V_s that is 2.5 times greater than that of the overlying soil layer and where the values of V_s of the underlying soil layers are all >400 m/s, H^* is defined as the depth above this layer. An expression for V_{se} is defined as follows:

$$V_{se} = d_0/t \tag{1}$$

$$t = \sum_{i=1}^{n} (d_i/V_{si}) \tag{2}$$

where d_0 refers to the smaller value between H^* and 20.0 m. Supposing there are n layers of soil according to the drilled borehole information, then d_i and V_{si} represent the thickness and the shear wave velocity for the i-th soil layer, respectively.

Engineering bedrock, as defined in Chinese seismic code, has a value of $V_s = 500$ m/s; however, it is softer than the NEHRP-defined rock layer that has a value of $V_s = 760$ m/s. Additionally, the computation depth for V_{se} is within 20 m, which is shallower than the value of 30 m commonly associated with the use of V_{S30}. Owing to the differences in site class definition, the reference mean HVSR curves given in previous literature cannot be applied directly to site classification in China. Therefore, the first task in this paper was to derive empirical reference HVSR curves that could be utilized as classification patterns for GRNN scheme.

2.2. HVSR Curves for KiK-net Stations

The borehole depth of the KiK-net stations is sufficient to reach rock layers where V_s far exceeds 500 m/s, whereas the maximum borehole depth of K-NET stations is only 20 m. Therefore, the KiK-net stations were used for computation of the reference HVSR curves given that the value of H^* for soft sites such as III and IV sites (see Table 1) is probably >20 m. K-NET stations were used for validation of our classification scheme.

Of 664 KiK-net stations with borehole data information, 638 stations were classified according to the range of V_{se} and H^* (Table 1). The other 26 stations were not included in this study because their corresponding borehole information was incomplete and thus their site class could not be derived accurately. Overall, 91, 499, 40, and 8 stations were classified as belonging to the I, II, III, and IV site classes, respectively, as illustrated in Fig. 1. Among the 91 class I stations, 25 stations were classified as outcrop hard rock site class where the V_s value of the first layer exceeds 500 m/s. The distribution of V_s values for these 25 stations is illustrated in Fig. 1 using a boxplot. The IV sites refer to extremely soft sites where H^* exceeds 80 m, which is unsuitable for installation of strong motion observation stations according to Chinese seismic code. In addition, only 8 KiK-net stations were classified as IV sites, which is an insufficient number for deriving a mean reference HVSR curve with statistical significance. Therefore, the IV site class is not further discussed in this paper.
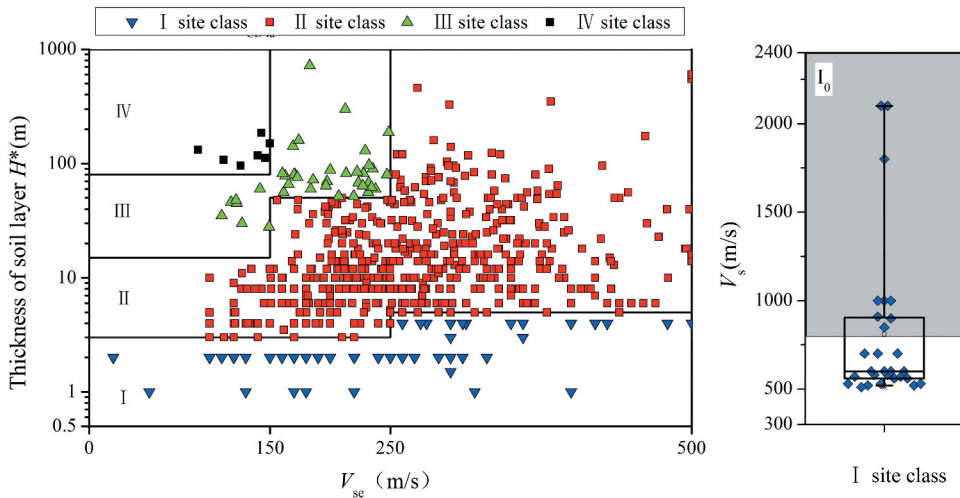
Figure 1. Site classification results for 638 KiK-net stations according to the range of the equivalent shear wave velocity of the sediment (V_{se}) and the thickness of the soil layer (H^*). The right boxplot indicates the distribution of V_s values of I sites where the first soil layer has a V_s value of >500 m/s. The I_0 sites that have a V_{se} value of >800 m/s are plotted in the area shaded gray.

A comprehensive Open-Source Site Database of Strong-Motion Stations in Japan was recently developed by Zhu et al. (2020a), which includes 1045 K-NET and 697 KiK-net site stations. This database contains site characterization parameters derived directly from available velocity profiles, including average wave velocities, bedrock depths, and velocity contrast. FAS is preferred over pseudo-spectral acceleration in detecting the site resonant frequency following the recommendations by Zhu, Cotton, and Pilz (2020b). After processing with an acausal Butterworth filter at cutoff frequencies of 0.1 and 30 Hz, the Fourier amplitude spectrum (FAS) of each recording in the database is calculated using the complete waveform. The S-wave is not selected to avoid the possible subjective impact caused by picking the S-wave window. The FAS is smoothed using the Konno–Ohmachi window with a smoothing coefficient of b = 20 (Konno and Ohmachi 1998). For a given record, the HVSR is computed as the geometric mean of the smoothed FAS of each of its two horizontal components divided by the smoothed FAS of its vertical component. In many applications, such as using machine learning for studies of site effects, it is essential to make the training dataset freely accessible. Therefore, all HVSR curves for the KiK-net and K-NET stations were calculated and compiled in the comprehensive ready-to-use site database

Before deriving the empirical reference HVSR curves, it is necessary to exclude those stations of which the HVSRs are without a "significant peak." For such sites, the predominant peak of the HVSR is difficult to identify and thus can easily be misclassified in practice (Alessandro et al. 2012; Fukushima et al. 2007; Ji, Ren, and Wen 2017). In Zhu et al. (2021), an automatic peak-recognition scheme was proposed based on the following three selection criteria, as illustrated in Fig. 2a:

(1) Significance: amplitude of peak exceeds a global threshold: $\max(c_1, c_2 + \log 10(\overline{HVSR}))$;
(2) Prominence: height of the isolated peaks > c_3;
(3) Sharpness: prominence/half-width of isolated peaks > c_4.

In Zhu et al. (2021), coefficients c_1 and c_2 are set as $\log_{10}(2.2)$ and $\log_{10}(1.4)$. In addition to significance criteria, the prominence and sharpness criteria are used to define the clarity of a peak relative to its neighboring points. The prominence (height of the isolated peaks) threshold value c_3 is set to $\log_{10}(1.8)$. The sharpness (prominence/half-width of isolated peaks) criterion is used to exclude broad peaks that arise owing to lateral variation in soil properties (e.g., Woolery and Street 2002), and
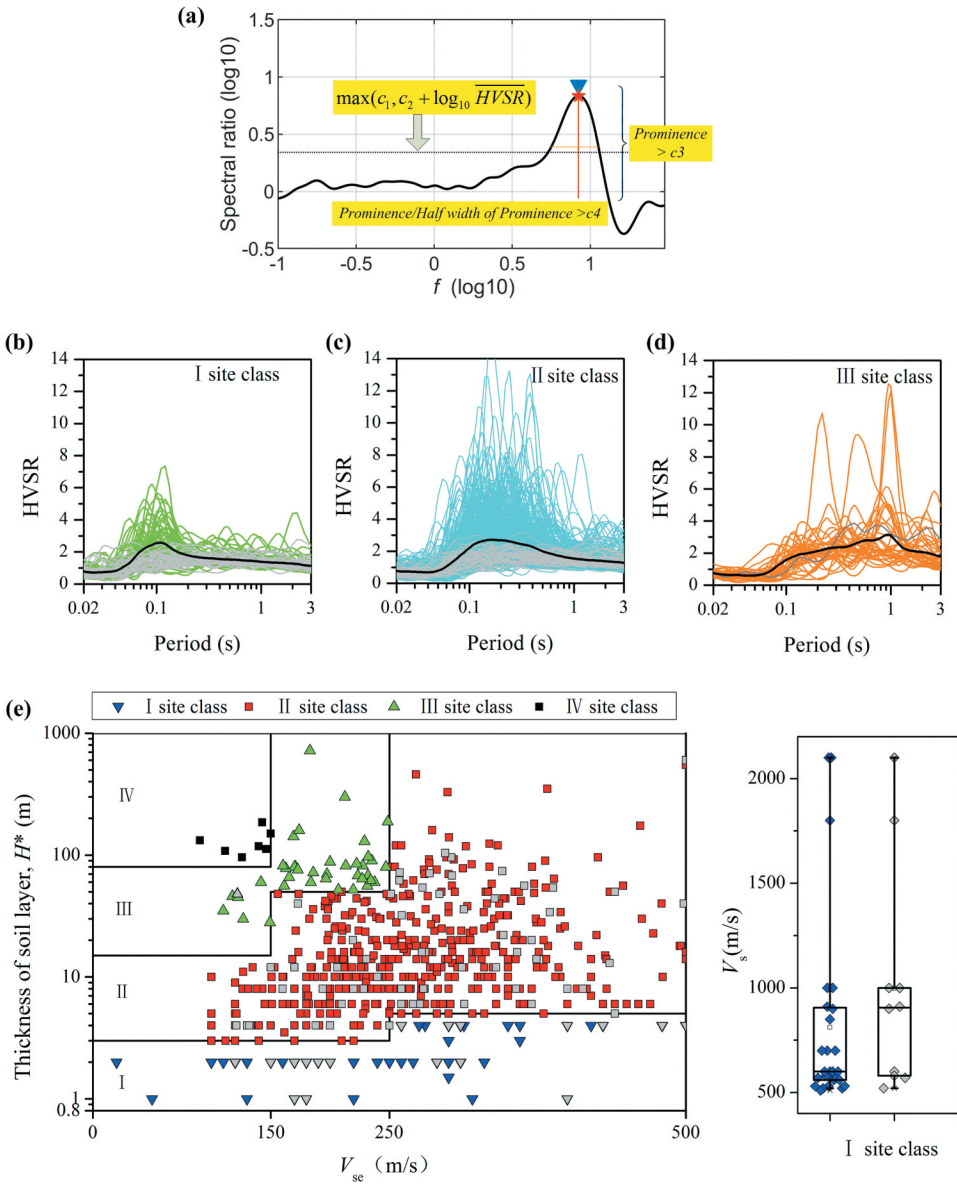
Figure 2. (a) Three criteria for detection of predominant or significant peaks in the HVSR curves (Zhu et al. 2021). The threshold values are labeled in the figure. (b)–(d) Individual HVSR curves and the corresponding arithmetic mean curves for the I, II, and III sites respectively. The gray lines represent the individual HVSR curves without a significant peak. (e) Distribution of V_{se} and H^* between sites with and without significant peaks, which are illustrated using different colors.

its threshold value is set as $c_4 = 0.5$. It is worth noting that the threshold values are not fixed and that other values might also be acceptable. The selection of the threshold values for peak recognition depends on user judgment. In our study, we needed only to detect whether significant peaks existed; therefore, accurate recognition of peaks in the HVSR curves was not essential for site classification. Ultimately, we decided to utilize the default threshold values recommended by Zhu et al. (2021). The script of the program for HVSR peak identification is freely accessible in the attachment files of the database (Zhu et al. 2020a).

Individual HVSR curves and the corresponding arithmetic mean curves for three sites are illustrated in Fig. 2b–d. There are sufficient recordings included for derivation of H/V curves of each KiK-net station. Therefore, the mean H/V curve of each station is very smooth. For I and II site class, there is basically no fluctuation in the reference curves. For III sites, slight fluctuation was observed in the period range from 0.1 s to 1.0 s because of the relatively small number of stations. As represented using gray lines, the HVSR curves of 31, 57, and 1 station for I, II, and III sites, respectively, were identified as without a significant peak. An HVSR curve might be relatively flat with no predominant peak for sites of rock or stiff soil, which explains why almost 1/3 of the stations of I site class were identified as having an HVSR curve without a significant peak. Owing to the complex soil properties and uncertainty in the HVSR curves, there were also no predominant peaks in the HVSR curves for 1/10 of the stations of II sites. The V_{se} and $H^{\star}$ for these excluded stations are annotated in Fig. 2e. There is no obvious V_{se} and $H^{\star}$ tendency or clear boundary that could be detected, i.e., these sites are distributed irregularly throughout the whole I and II site classes. These stations should not be included in an automatic site classification procedure and must be analyzed individually in practice. To ensure that the entire classification procedure is as succinct as possible, we decided to not implement the amplitude of the HVSR curves as one of the criteria for identification, as was performed in our previous study (Ji, Ren, and Wen 2017).

3. GRNN Site Classification Scheme

Before further introduction of our proposed site classification scheme, we briefly review the basic concept of the GRNN method (Specht 1990) that is typically constructed using four layers: the input layer, pattern layer, summation layer, and output layer (Fig. 3). The first layer is the input layer, which is fully connected to the second layer. There are n nodes in the first layer and each node represents an element in the input vector $\mathbf{X}\{X_1, X_2, X_3 \ldots X_n\}$, which is fully connected to all the neurons in the second pattern layer. The pattern layer consists of n nodes and each node is associated with the input vector assigned with the j-th sample in the training data. Each unit in the pattern layer implements a radial basis function by computing the Gaussian kernel of the Euclidean distance between the existing input vector and the training pattern. The outputs of the pattern units are passed to the summation layer and two types of neuron are constructed: S-summation neurons and D-summation neurons. The difference between these two types of neuron depends on whether weights defined from the training results are implemented in the outputs from the pattern layer. The final output layer then divides the output from the S-summation neurons by that from the D-summation neurons. The probability of the j-th pattern (P_j) for an unknown input vector $\mathbf{X}$ could be computed using Equations. (3) and (4)

$$D_i = (X - X_i)^T (X - X_i) \tag{3}$$

$$P_j = \frac{\sum\limits_{i=1}^{n} Y_j \exp\left(-\frac{D_i^2}{2\sigma^2}\right)}{\sum\limits_{i=1}^{n} \exp\left(-\frac{D_i^2}{2\sigma^2}\right)}, i = 1, 2, 3 \ldots n; j = 1, 2, 3 \ldots k; \tag{4}$$

where D_i is the Euclidean distance between the existing input vector and the training pattern, n is the number of elements concerned in input vector $\mathbf{X}$, and σ is referred to as the spread factor, which influences the results in the output layer of the GRNN. Y_j is the classification results index number.

Considering that our problem is to classify sites according to the shape characteristics of HVSR curves, the HVSR curve values at n different natural periods for the unknown sites were utilized to construct the input layer of the GRNN. The number of nodes in the pattern layer is equal to the number of natural periods of concern used in the input layer. Supposing that we have k site classes that need to be identified, the summation layer should have $k + 1$ neurons, i.e., k S-summation neurons and
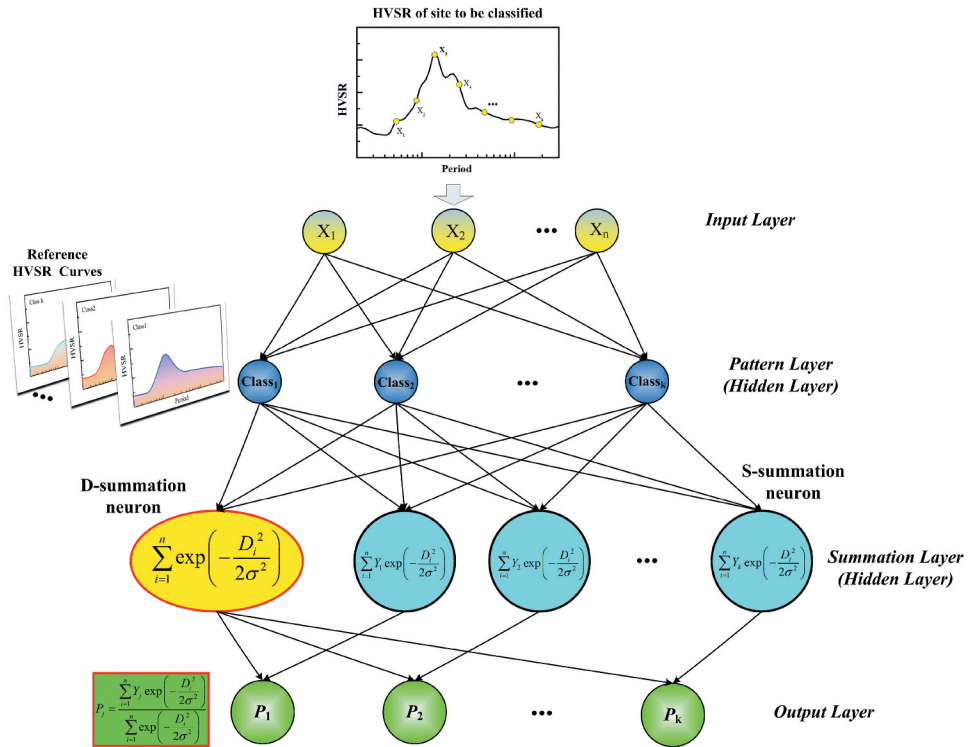
Figure 3. Typical four-layered structure of a generalized regression neural network. The input layer is constructed using the unclassified HVSR curves with *n* neurons representing the values at various periods in the HVSR curves. The reference curves of different site classes are used to build the pattern layer. Results from the output layer provide the corresponding probabilities for different site classes.

one D-summation neuron. The output layer of the GRNN model would then provide a *k*-node output, where the output of each node indicates the probability of a station belonging to different site classes. It is worth noting that we did not give the final continuous value in the range of [0,4] or [0,3] as in Yaghmaei-Sabegh and Tsang (2011). Supposing that we have probability results for I, II, II, III as P_1 = 0.3, P_2 = 0.1, P_3 = 0.1, and P_4 = 0.5 respectively. If the index number for them, Y_j, are defined as 1,2,3,4, the continual form of the GRNN results would be $0.3 \times 1 + 0.1 \times 2 + 0.1 \times 3 + 0.5 \times 4 = 2.8$, this would give us misleading results (IIb) considering that Class III have the largest probability. That is why we did not directly set the value of Y_j as 1,2,3,4 . . . for different site classes in the summation layer. For site class01, the Y_j is set as [1,0,0,0]; site class02, the Y_j is [0,1,0,0]; site class03, the Y_j is [0,0,1,0] . . . There is merit for this form of Y_k that no matter which code number the site class is defined, the final classification results, the site class with largest probability, would not be influenced. If the users want, however, they could easily derive the [0,3] or [0,4] continual form by multiplying [1,2,3,4.] with the corresponding probability from output layer.

Proper construction of the pattern layer is fundamental for solving the site classification problem. One possible way is to construct the pattern layer using all the HVSR curves for all the different site classes. However, the sample size of both the I and the III sites in our database was too small in comparison with that of the II sites, making it nearly impossible to build a stable pattern layer in this way. To overcome the problem of unbalanced samples sizes, we tried various methods that included oversampling and undersampling techniques; however, the classification results were unsatisfactory because of the potential overfitting or underfitting phenomenon. Therefore, the average curves of the HVSR curves relating to the different site classes were used directly as the pattern layer rather than including all the individual HVSR curves. However, this operation made the final site classification

results very sensitive to the reference HVSR curves themselves, as is discussed in Section 5. In the future work, we want to include more parameters, like station elevation, geology and topographic data to settle this problem.

Another problem is whether normalization of the HVSR curves should be performed. Although normalizing the input data and the pattern layer in an artificial neuron network is usually necessary for numerical or convergence reasons. If variables are measured on different scales, the effect of variables with small scale might be submerged in the variables with larger scale, which would produce incorrect results. Using normalization would also help the gradient of the neural network decreases faster. However, it might be unnecessary for our problem because the pattern layer was constructed using three reference curves rather than using a large training dataset. Thus, normalization would not be required to improve the network training performance. More importantly, the difference between the peak amplitude of the HVSR curves relating to the different site classes would not be identifiable if normalization were performed. In Section 5, the performance of the GRNN method when adopting normalization of the HVSR curves is compared to that without normalization.

For the GRNN method, there is no need to define training parameters such as the learning rate used in an error backpropagation neural network. Another similar and widely used pattern classifier is the probability neuron network (PNN) (Specht 1990), in which the final layer is the competitive layer that only provides output values in discrete form. The advantage of the GRNN method is its ability to produce continuous output values for different site classes that represent the probability that the HVSR is identified for the corresponding site class. The σ in Equation (4) is referred to as the spread factor, which was set as 1.0 in the previous study (Yaghmaei-Sabegh and Tsang 2011). As we used the reference curves of the different site classes directly to construct the pattern layer, the choice of the spread factor does not substantially influence the final classification results, which have the greatest probability. However, the specific probability values derived for different site classes are not constant under different spread factors. The smaller the spread value, the more likely the probability for each site class will be 0.0 or 1.0 rather than any intermediate value. A user could define a minimum probability threshold value (ranging from 0.0 to 1.0) to exclude any HVSR curve with shape characteristics similar to two or more site classes. Supposing that the probability is larger than the threshold value, then the corresponding site class was selected for the target station. The threshold value should not be set too large or too small, and we set the threshold value as 0.5 in our study. If the threshold value was set too large, a large number of sites with HVSR curves similar to two or more types of classes would not be detected. Conversely, if the threshold value was set too small, a large number of stations would fail the classification process because of the strict limit.

A flowchart of the process of the GRNN-based site classification scheme is presented in Fig. 4. The process involves the four following steps:

Step1: For an unknown site that needs classification, check whether significant peaks exist in its HVSR curve. If there are no peaks, the site cannot be classified using our scheme.
Step2: Use the reference HVSR curves to build the GRNN network.
Step3: Compute the probability values for different site classes.
Step4: Compare the maximum probability with the predefined threshold value and determine the final site class. Here, the default threshold value was set as 0.5.

4. K-means Clustering for II Sites

Of the 539 classified KIK-net stations, the majority (441) belong to the II site class because of the wide range of the values of V_{se} and $H^{\star}$, as illustrated in Fig. 2e. As it is unrealistic to use a single mean curve to represent the HVSR characteristics of this class, it was necessary to separate the HVSR curves of the II sites into more than one reference curve.
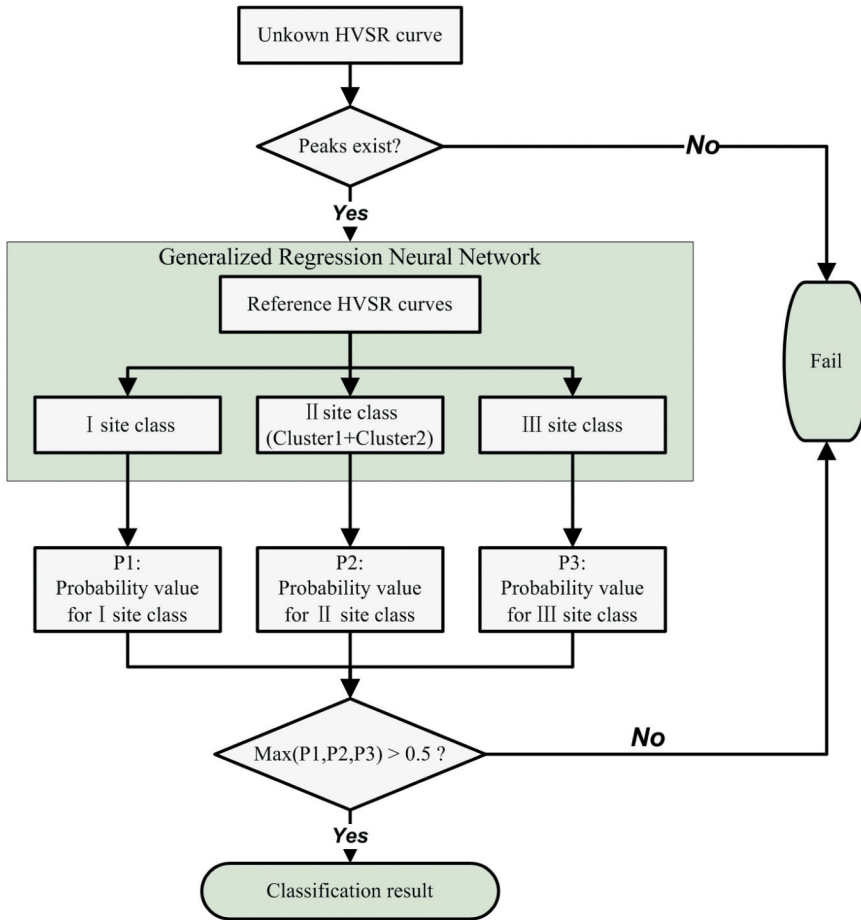
Figure 4. Flowchart of the process of the GRNN-based seismic site classification scheme.

Clustering analysis is the process of categorizing unlabeled observation data into clusters or groups according to their degree of similarity. The K-means clustering approach, which is the method used most commonly for clustering analysis in machine learning and data mining work, assigns each observation point into a cluster by minimizing the distance from the observation to the center of the corresponding cluster. It is an unsupervised classification procedure because no standard reference models or curves are predefined as in the traditional empirical classification procedure. In recent seismic site effect studies, K-means clustering has been used successfully on many occasions in applications such as nonlinear site response recognition and categorization of the site amplification function (Ji et al. 2020; Kotha, Cotton, and Bindi 2018; Zhu, Pilz, and Cotton 2020c). The unsupervised K-means clustering algorithm was applied in our study to further separate the HVSR curves of the II sites into subgroups.

Determination of the optimal clustering number must be accomplished before K-means clustering is applied. As the optimal clustering number is the only information provided in the unsupervised clustering analysis, it has considerable influence on the clustering results. There are two methods commonly used for the estimation of optimal clustering number. One is the F-stopping-rule index of Caliński and Harabasz (1974), which is determined by the within-cluster and between-cluster sum of the squared errors. The larger the Caliński–Harabasz index, the greater the difference between clusters and the more likely it is to be selected as the optimal cluster number. The clustering number is in the range of 2 to 10 and the corresponding values of the Caliński–Harabasz index are
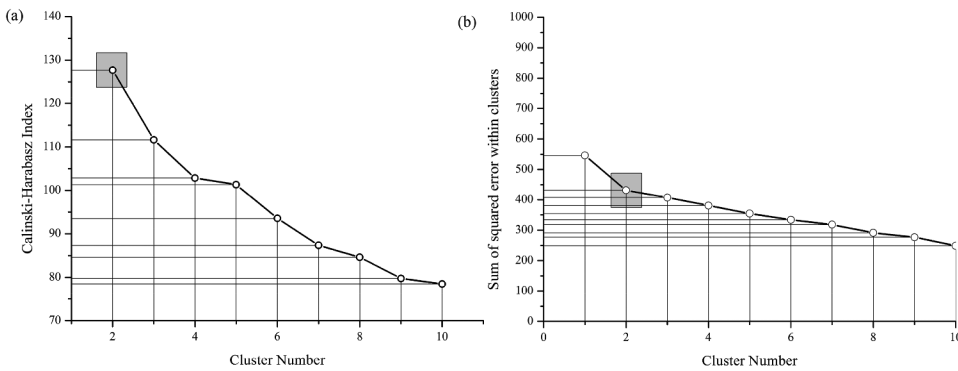
Figure 5. Relationship between clustering number and (a) the Caliński–Harabasz index and (b) the sum of the squared error within clusters.

plotted in Fig. 5a. It can be seen that the largest value of the Caliński–Harabasz index occurs when the observations are divided into two clusters. The other popular method involves using the change of the slope of the sum of the squared error (SSE) within different numbers of clusters. As the clustering number increases, the number of observations in each cluster decreases, which results in the reduction of the SSE. When the SSE decreases slowly after a specific number of clusters, further increase in the number of clusters will not significantly improve the clustering performance. Therefore, we treated the "elbow" location in the slope of the SSE as the optimal number of clusters. As illustrated in Fig. 5b, the "elbow" of the SSE curve exists when the observations are separated into two clusters. After evaluation of different clustering numbers using these two methods, it is found that two clusters were optimal, resulting in the smallest SSE without introducing large overlaps among the clusters.

Considering that the purpose of the clustering algorithm in this study was to determine the reference curves for the II site class, it was necessary to ensure that the arithmetic mean curves of the different clusters in the II site class were dissimilar to the reference curves for the I and III site classes. For comparison, we separated the II observations into two and three clusters using the K-means algorithm, as illustrated in Fig. 6a and b, respectively. The arithmetic mean curves of the different clusters are compared with the results for the I and III site classes. As can be seen from Fig. 6d, if the II sites were divided into three site clusters, the mean curve of the IIa cluster would be very similar to the I reference curve, which would inevitably undermine the performance of the GRNN site classification method. However, if the II HVSR curves were separated into two clusters, significant difference remained between the I and III mean curves (Fig. 6c).

Next we would use the non-parametric Kruskal–Wallis test to evaluate whether the H/V curves separated by K-means method are statistically different. Because the data in our study does not always meet the normality assumption and the sample size is not large enough, Kruskal–Wallis test rather than one-way ANOVA (analysis of variance) were utilized. For a specific period, the null hypothesis is that the H/V value of each groups comes from the same distribution; The alternative hypothesis is that not all groups come from the same distribution. We calculated the corresponding p-value for period ranging from 0.02 s to 6.0 s, as shown in Fig. 7. Supposing that the significant level is 0.1, it can be seen that the difference among classes are significant from 0.04 s to 4.0 s when II site class is separated into two clusters using the K-means clustering algorithm. Only in short period (less than 0.04 s) and the long period (4.0 s to 5.0 s), we accept the null hypothesis that the H/V value of each groups comes from the same distribution which would not significantly influence the classification results. On the other hand, the p-value for I and IIa site class exceeds 0.1 for period range from 0.01 s to 2.0 s, accepted the null hypothesis that they are from same distribution. The difference between three clusters are not significant as two clusters either. The comparison results indicate that two clusters are more wise
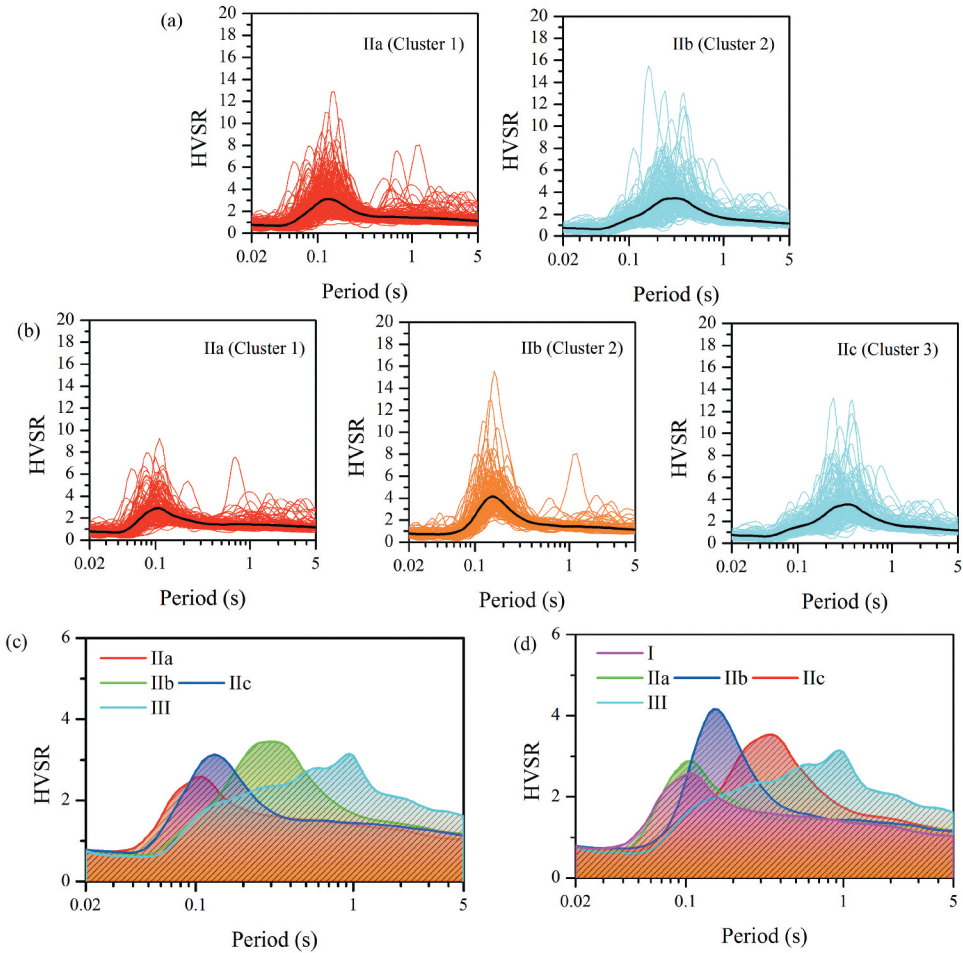
Figure 6. The II site class separated into (a) two and (b) three clusters using the K-means clustering algorithm. (c) (d) Comparison between the mean curves of the I, II, and the III site classes. (c) refers to two clusters and (d) refers to three clusters.

choice considering the reference curves' difference is more significant among different classes. Therefore, the II sites were separated into two clusters, which were used to construct the two corresponding reference curves.

5. Validation of the Proposed Classification Scheme

5.1. Site Classification for KiK-net Stations

Before utilizing the method (Fig. 4) for site class identification in China or other regions, it was necessary to evaluate the classification performance regarding the same selected KiK-net stations. The input layer of the GRNN model was designed with 94 nodes, representing corresponding HVSR values at natural periods in the range of 0.02–5.0 s with logarithmically evenly spaced intervals. As illustrated in Table 2, four cases were considered in this study to determine whether to apply normalization for the reference and whether to use K-means clustering for the II class.

For cases No. 01 and No. 02, the reference curves for different site classes were normalized using Eq. (5)
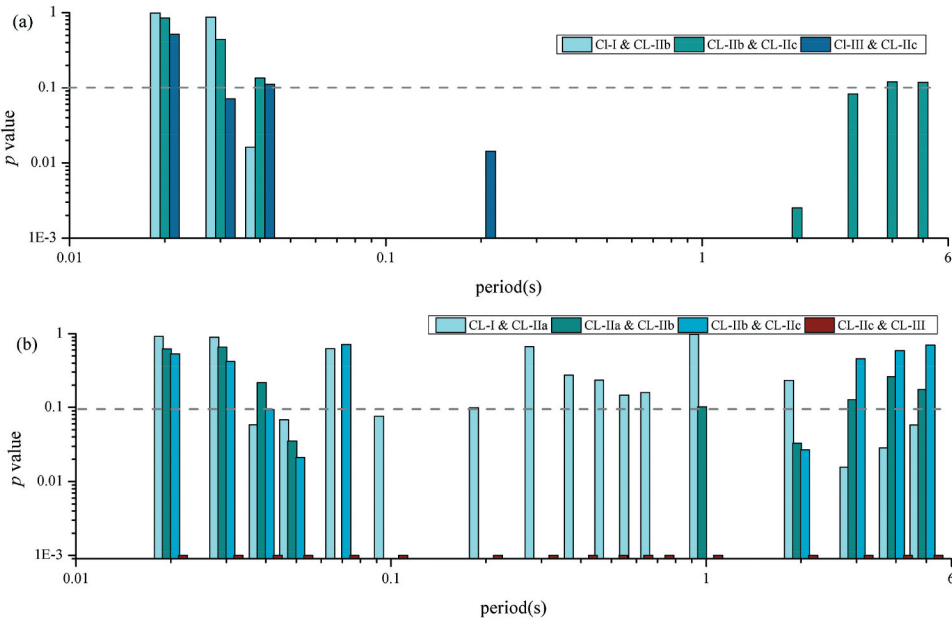
Figure 7. The *p*-value calculated using Kruskal-Wallis test for the null hypothesis that the H/V ratio, ranging from 0.02s to 6.0s, comes from the same distribution regarding (a) two clusters and (b) three clusters.

Table 2. Four cases of concern in this study.

Case Code	Apply Normalization?	K-means Clustering for II site class?
No.01	Yes	No
No.02	Yes	Yes, using reference curves of 2 clusters
No.03	No	No
No.04	No	Yes, using reference curves of 2 clusters

$$HVSR_i^{normalized} = \frac{HVSR_i - \min(HVSR)}{\max(HVSR) - \min(HVSR)} \tag{5}$$

The individual HVSR curves for each station were also normalized using the same equation. For cases No. 02 and No. 04, the reference curves for the II class were derived from the mean HVSR curves of the K-means clustering results, as illustrated in Fig 6a. The probability for the II class was the sum of the probability regarding the IIa and IIb classes. The references curves and the GRNN classification results for the four cases are compared in Fig. 8. For case No. 01, a large number of stations were classified as the I class for all three types of site class. Fewer than half the II sites were identified correctly. The classification performance in case No. 03 was much better than in case No. 01, i.e., more than half the sites were assigned to the right class. Considering that the only difference between these two cases was the application of normalization, it is proven that the choice to not apply normalization is better in relation to Chinese seismic site classification. The comparison between cases No. 01 and No. 02 illustrates that classification performance could be improved significantly by applying K-means clustering for II sites. The same phenomenon can be observed between cases No. 03 and No. 04, especially for the classification results of II sites. The successfully classified results in case No. 04 are balanced regarding different site classes, indicating reasonably stable and robust performance.

The classification results among the four different cases are illustrated in Fig. 8; however, their relative classification performance must be evaluated and compared objectively. For this purpose, the Receiver Operating Characteristic (ROC) curve is introduced, which involves plotting the true positive
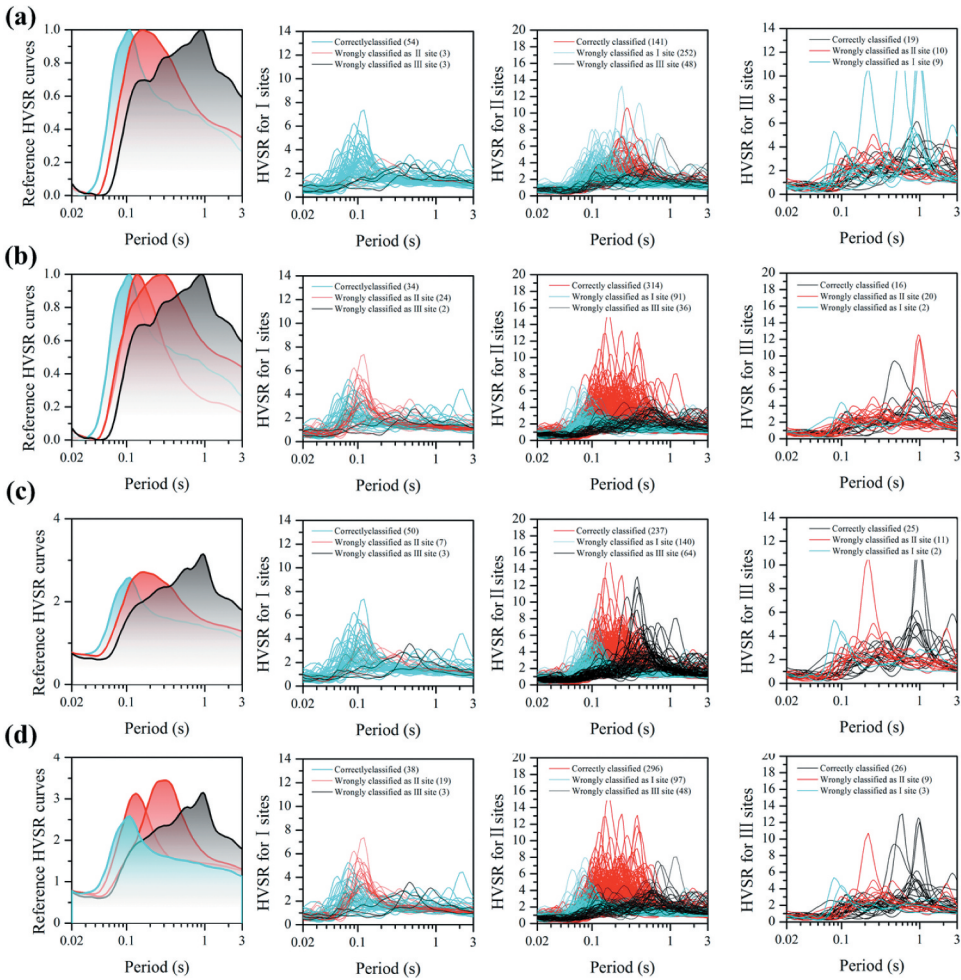
Figure 8. Reference HVSR curves for the GRNN and the site classification results for I, II, and III stations in KiK-net conditioned under case (a) No. 01, (b) No. 02, (c) No. 03, and (d) No. 04. For cases No. 01 and No. 02, the reference curves for different site classes were normalized using Eq. (5). For cases No. 02 and No. 04, the reference curves for II were derived from the mean HVSR curves of the two clusters.

rate (TPR) against the false-positive rate (FPR). The TRP is the proportion of observations predicted correctly to be positive out of all positive observations, i.e., true positive/(true positive + false negative). The FPR is the proportion of observations predicted incorrectly to be positive out of all negative observations, i.e., false positive/(true negative + false positive). Taking the prediction of the I site class as an example, a positive case is when the station is classified as belonging to the I site class, whereas the negative case is when the station is classified as belonging to either the II or the III site class. The TPR is the proportion of HVSR curves classified correctly as relating to the I site class among all the predicted I sites, while a false positive represents the situation in which the II and III stations were identified incorrectly as I sites. The FPR is the proportion of HVSR curves classified incorrectly as relating to the I site class among all the II and III sites. In a ROC curve, a higher X-axis value indicates a higher number of false positives than true negatives. As the ROC curve shows the trade-off between sensitivity (or the TPR) and specificity (1 − FPR), the classifiers that produce curves closer to the top-left corner indicate better performance. The area under the ROC curve, which is abbreviated to AUC, is the index used most widely for description of classifier performance. The higher the AUC, the better the classifier performance in distinguishing between positive and negative classes. For the case

AUC = 1, the classifier is perfect and could predict all classes correctly. For the case 0.5 < AUC < 1, the classifier tends to identify more true positives and true negatives than false negatives and false positives. For the case AUC = 0.5, the classifier is unable to effectively distinguish between different classes, because it is equivalent to a random prediction of class. Therefore, better classifiers tend to have higher AUC values. In our problem, the ROC curve for class I is generated by classifying I against not I, i.e., II or III. Similarly, the ROC curve for class II (III) is generated by classifying II (III) against not II (III).

The ROC curves and the AUC values for the four cases (Table 2) were computed and are illustrated for comparison in Fig. 9. The ROC curves of all four cases lie on the left upper side of the boundary line with AUC = 0.5, while differences can be observed between the AUC values relating to the four specific cases. The AUC value of the II site class regarding case No. 01 (i.e., 0.693) is the lowest of all four cases. If K-means clustering for II sites was applied (as in case No. 02), the AUC values of the II site class would increase to larger than 0.73. If normalization was not applied (as in case No. 03), the AUC value would increase further to 0.759. For case No. 04, with K-means clustering and without normalization, the AUC value of the I site class was slightly lower than that in case No. 03, while the AUC values of the II and III site classes were the largest among all four cases. Therefore, we confirm that the performance of case No. 04 was best overall and that the proposed classification scheme is plausible.

More than 80% of the studied stations are classified as II sites according to their borehole information. The total accuracy rate cannot comprehensively evaluate the overall site classification performance for all three site classes, which would potentially be influenced by the rate of success for the II sites. Therefore, a confusion matrix is introduced for subjective description of the performance of the classification model. As illustrated in Table 3, elements x_{ij} in the confusion matrix (i is the row index number and j is the column index number) indicate those cases belonging to class
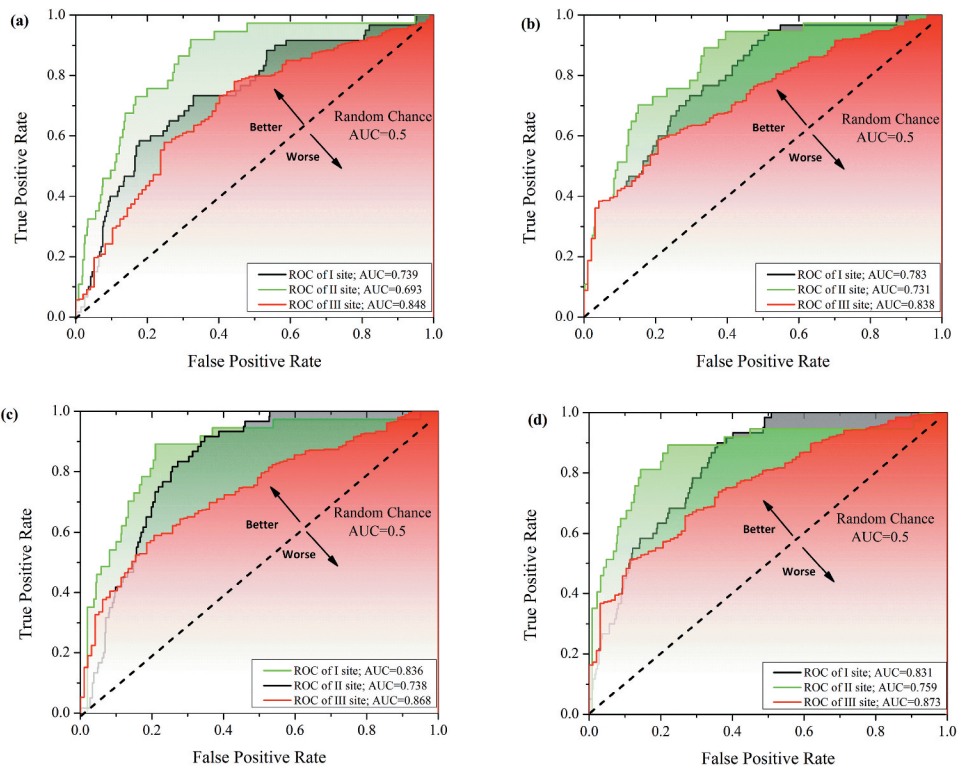

Figure 9. ROC curves for the four studied cases((a) Case01, (b) Case02, (c)Case 03, (d)Case04) regarding classification of the three site classes. The AUC values representing the area under the ROC curve for each site class are listed in the legend.

Table 3. A confusion matrix table for the GRNN site classification results regarding KiK-net stations.

Prediction Site Class	Actual Site Class			Precision rate
	I	II	III	
I	40	97	3	28.60%
II-Cluster1	18	155	0	91.10%
II-Cluster2	2	143	9	
III	0	46	26	36.10%
Recall rate	66.60%	67.57%	68.42%	
Overall Accuracy Rate		67.53%		

j that were classified as class *i*. Hence, the elements in the diagonal are those classified correctly, whereas the elements out of the diagonal are those misclassified. The precision rate quantifies the number of site class predictions that actually belong to the corresponding site class. The recall rate for a specific site class was calculated using the proportion of correctly classified stations out of the total number of stations in the corresponding site class. The overall accuracy rate quantifies the total number of correct predictions among all example observations. As can be seen from Table 3, the precision rate is influenced significantly by the unbalanced sample size of the observations for the different site classes. Owing to the large number of II sites, the precision rate for the II site class is 91.10%, which is markedly larger than the values of 28.60% and 36.10% for the I and III site classes, respectively. The recall rate is not influenced by the different sample sizes of the site classes and is better able to objectively reflect classification performance, which for the I, II, and III site classes is 66.6%, 67.57%, and 68.42% respectively. In our study, we did not implement the amplitude of the HVSR curves as one of the criteria for identification as explained before. If we did not exclude the flat H/V curves and assigning the H/V curves with amplitude less than 2.2 as the I site class. The recall rate for I site class would increase from 66.6% into 76%, while the recall rate for II site class decrease from 68% into 63%.

The accuracy rate (recall rate) of the site classification results using different methods were compared by Ji, Ren, and Wen (2017). The recall rate for method proposed in Ji, Ren, and Wen (2017) are 64%, 62% and 58% regarding I, II, and III site classes. For method proposed by Zhao et al. (2006), I and III site classes are classified with a recall rate nearly 70% while the success rate is only 25% for II site class. The performance of method proposed by Ghasemi et al. (2009) is relatively better for CL-II sites (success rate of 63%) than for CL-III (46%) and CL-I (33%) sites.

5.2. Site Classification Scheme Validation Using K-NET Data

The K-NET stations were used to further validate the applicability of the classification scheme using a different dataset. As the maximum drilled borehole depth of K-NET stations is 20 m, some of the II, III, and IV sites could not be identified according to borehole information, as illustrated by the shaded pattern in Fig. 10. Only one station was classified as a III site, and II sites at which the depth of the soil thickness is >20 m could also not be identified. Classification results might jump from one class into another class owing to slight changes in the values of V_{se} and H^* if they lie exactly on the boundary. As is known, uncertainty in drilled borehole information is prevalent and this problem could not be neglected. To prevent its potential impact from spreading into the evaluation of the performance of site classification for I and II sites, 39 stations that lie exactly on the boundary were excluded from the validation. Additionally, stations at which the V_s value of the bottom soil layer at depth 20 m was <500 m/s were also excluded because the sediment depth could not be measured accurately. The gray symbols in Fig. 10 represent excluded stations without predominant peaks in their HVSR curves,
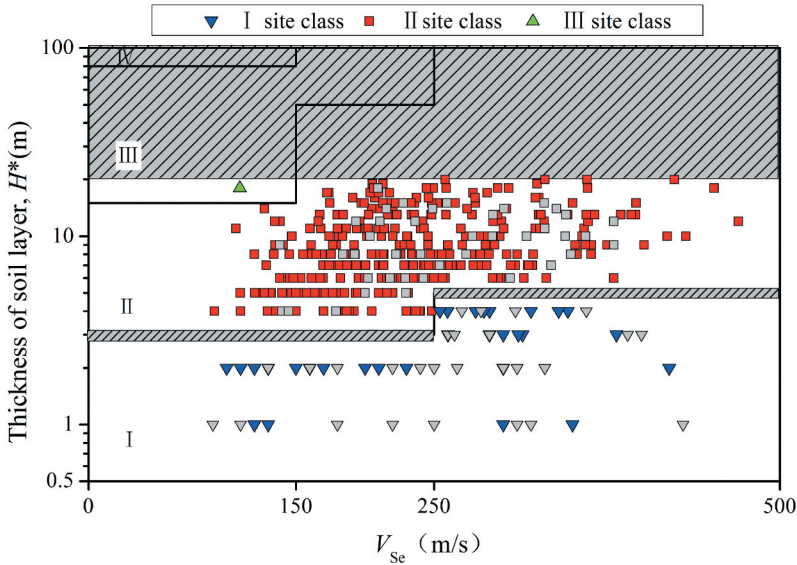
Figure 10. Distribution of the values of V_{se} and H^* for the studied K-NET stations. Sites with sediment thickness > 20 m could not be identified owing to the borehole depth limit, as illustrated by the hatched shaded pattern. Stations that lie exactly on the boundary of the I and II site classes were also excluded. Sites without predominant peaks in their HVSR curves are represented by gray symbols.

according to the criteria mentioned in Section 2.2. Ultimately, 330 K-NET stations were selected for validation of the GRNN site classification scheme with 35, 294, and 1 station identified as I, II, and III site classes, respectively.

A confusion matrix for the K-NET classification results was computed and the results are listed in Table 4. It can be seen that the recall rates for I and II site classes are 68% and 60%, respectively, and that the overall accuracy rate is 61.0%. The classification performance for I sites is similar to that of the KiK-NET stations. However, the recall rate of the classification results for the II sites is relatively lower than that for the KiK-net stations, which is likely because almost half the II stations were excluded owing to the borehole depth limit. The performance of matching III site class were not validated because only one sample data was included.

We calculated the mean HVSR curves for all the classified K-NET sites and then compared them with the reference curves used in our GRNN scheme, which were derived from the KiK-net dataset. As illustrated in Fig. 11, the three mean HVSR curves have shapes similar to the reference curves. The predominant period of the mean curve of the I site class is slightly shorter than the reference curve. The mean II site class HVSR curve lies exactly between the reference curves of the two clusters relating to the II sites. The curve for the III sites is almost the same as the III reference curve. The validation results indicate that the GRNN site classification scheme could be applied effectively in the evaluation of soil conditions.

Table 4. A confusion matrix table for the site classification results regarding K-NET stations.

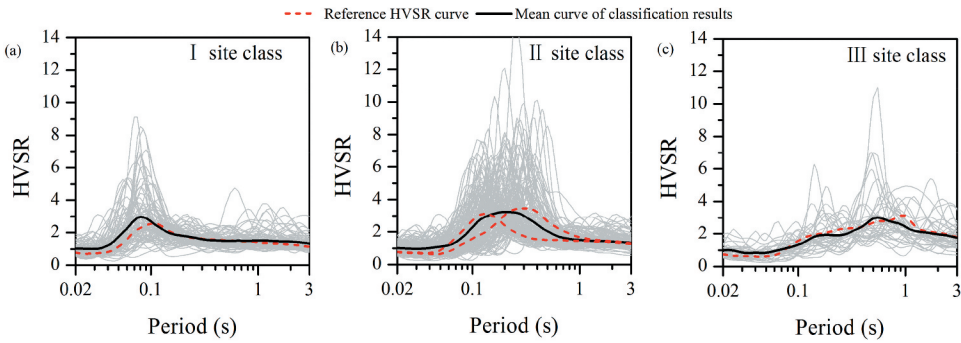| Prediction Site Class	Actual Site Class			Precision rate
	I	II	III	
I	24	71	0	25%
II	9	176	0	95%
III	2	47	1	–
Recall rate	68%	60%	–	
Overall Accuracy Rate			61.0%	

Figure 11. Comparison between the reference curves and mean HVSR curves derived from the classification results of 330 K-NET stations.

6. Application of the GRNN Site Classification Scheme to China Stations

6.1. NSMONS Strong Ground Motion Data Set

The strong ground motion dataset used here is largely the same as that utilized in our previous HVSR site classification work (Ji, Ren, and Wen 2017). Overall, 7183 three-component recordings were extracted from the China National Strong Motion Networks Observation Center (2007–2015). After excluding recordings from the Wenchuan and Lushan earthquake events, the remaining recordings were processed and the corresponding HVSRs were computed using the procedure discussed in Section 2.2. We used the recordings with peak ground acceleration in the range of 5–100 gal to avoid possible influence from recordings with a low signal-to-noise ratio and site nonlinearity response under strong ground motion input. Only stations with more than three recordings were selected to ensure that stable HVSR curves could be obtained. Ultimately, 200 stations with 1281 recordings were selected for site classification in China.

6.2. Site Classification Results

Using the GRNN site classification scheme, 167 of 200 NSMONS stations were classified. No significant peaks could be identified in the remaining 35 stations according to the criteria mentioned in Section 2.2. Of the 167 stations selected, 32, 88, and 47 stations were classified as I, II, and III site classes. The corresponding probability for each site class and the final classification results are listed in Table A1.

The average HVSR curves were calculated for I, II and III site class according to the site identification results. Then the mean curves were compared with the reference curves derived from the selected KiK-net data as illustrated in Fig. 12. For all classes, the overall shapes of the derived mean curves are similar to the target reference curves, indicating that the classification results are generally satisfactory. For I sites, a predominant peak cannot be identified in the mean curve, which might reflect the small number of classified I stations (32 stations) in China.

We collected borehole information of 73 classified stations using drilling P-S logging data from station construction reports, and we calculated the corresponding V_{se} and $H^{\star}$ to classify the site classes based on the definition of Chinese seismic code. The distributions of the values of V_{se} and $H^{\star}$ are presented in Fig. 13. The V_{se} and $H^{\star}$ information could be found in Table A2. Most HVSR-classified stations are consistent with the results derived from borehole data. Owing to the wide range of values of V_{se} and $H^{\star}$, the recall rate for the II site class is almost 100%. For some stations, the borehole depth only reaches 20, 30, or 50 m, and the actual sediment thickness is not measured. They were labeled exactly on the boundary of 20, 30, or 50 m in Fig. 13. It is possible that if the actual soil layer thickness was >50.0 m, these stations might be classified as III site class. In the coastal area of Tianjin Province, the sediment thickness at some stations is >50 m (i.e., 012DAT,
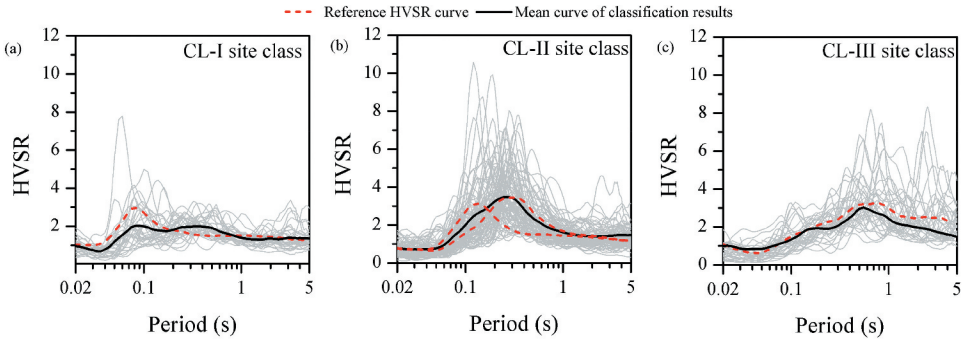
Figure 12. Comparison between the reference curves and mean HVSR curves computed based on the GRNN classification results of the NSMONS stations. Overall, 32, 88, and 47 stations were classified as I, II, and III site classes.
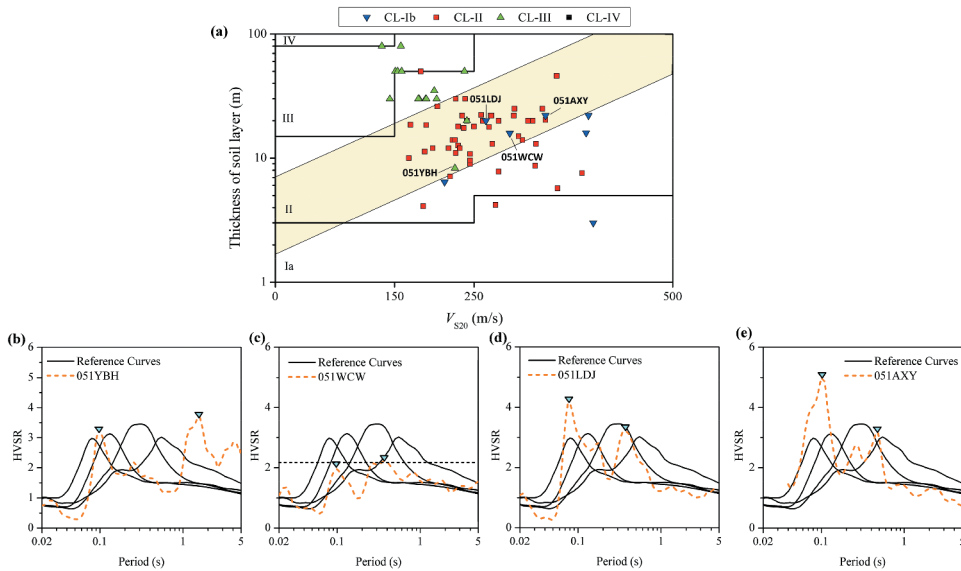

Figure 13. Comparison of site classes based on borehole data and assigned using the GRNN-based HVSR method for some NSMONS stations.

012DZZ, 012FTZ, 012XAZ, and 012ZHB). These stations with soft site condition were all assigned successfully to the III class using the GRNN scheme. Three stations (051MXD, 053RHT, and 065WSL) were treated as "rock" stations based on geological investigation before selecting the station location. They were all assigned successfully to the I class using the GRNN classification scheme. Among the 32 stations classified as I site class, the borehole information of 7 stations indicated that they were II sites. Borehole data of six stations classified as III site class indicated that they were actually II sites, partially because the depth of their soil layer (>30 m) is close to the boundary between II and III sites. We plotted the H/V curves for four mis-identified stations in central parts of the clusters of the class II, as shown in Fig. 13b–e. 0.51YBH was wrongly assigned with CL-III site class mostly because there are more than one peaks observed in the H/V curves. The peaks at long period around 1.0 s makes it wrongly assigned with the CL-III site class. Same phenomenon was observed for all three mis-identified CL-II stations that there are more than one predominant peaks in the H/V curves. The predominant peaks at short period around 0.1 s makes

them wrongly assigned with the CL-I site class. For 051LDJ, the amplitude of H/V curve is 2.23, which is slightly exceeds our predefined amplitude threshold. It is indicated that the H/V curves with multiple peaks would influence the GRNN matching results. Considering that the overall accuracy rate of the GRNN scheme is around 60% to 70% for the KiK-net and K-NET stations, similar classification performance is expected for NSMONS stations, according to the borehole validation results of the 73 stations.

7. Conclusions

In this study, we developed the GRNN method in HVSR seismic site classification. China strong motion stations were used as example study case.

Firstly, the HVSR curves of 539 KiK-net stations in Japan were selected for construction of reference patterns. To reduce the variability within specific site classes, K-means clustering algorithm was proposed to further separate the HVSR curves of II site class stations into two patterns. The ROC curve and AUC computation results indicated that non-normalization and K-means clustering for II sites could improve the overall classification performance for all three site classes. After exclusion of the HVSR curves without predominant peaks, the overall recall rate for I, II and III sites could reach 66.60%, 67.57%, and 68.42% respectively. This is proved to be an efficient strategy for site classification which having relatively wide parameter boundary range. The GRNN-based classification scheme was then validated using borehole information of 330 K-NET stations, which resulted in a recall rate of 68.0% and 60.0% for I and II site classes, respectively. The mean curves of the classified stations were similar to the reference curves that were used in the pattern layer. Considering that almost half the II site class stations were not included in the validation owing to the maximum borehole depth limit of K-NET stations, the classification performance was reasonably satisfactory.

Finally, based on the HVSR curves calculated from China strong ground motion data acquired during 2007–2015, the site conditions of 167 NSMONS stations were estimated using the GRNN-based classification scheme. The results were partially validated using borehole information from 73 stations. The degree of similarity between the mean curves of the classification results and the reference curves indicated that the classification results were reasonably reliable.

The proposed GRNN-based site classification scheme represents a promising method for estimation of the site conditions according to Chinese seismic code. This would be helpful for accurate analysis of ground motion data in China and could be applied further regarding development of ground motion models. The proposed site classification workflow could also be applied to other regions or countries after proper adjustment of the reference HVSR curves according to different site class definitions.

Disclosure Statement

No potential conflict of interest was reported by the author(s).

Data And Resource

The script of GRNN site classification scheme in this study and established reference curves are free to download from Github. (https://github.com/JIKUN1990/GRNN-Seismisite-classification-HVSR-JK1.0).

Funding

ORCID

Kun Ji 🆔 http://orcid.org/0000-0003-0314-5216

References

Alessandro, C. D., L. F. Bonilla, D. M. Boore, A. Rovelli, and O. Scotti. 2012. Predominant-period site classification for response spectra prediction equations in Italy. *Bulletin of the Seismological Society of America* 102 (2): 680–95. doi: 10.1785/0120110084.

Building Seismic Safety Council (BSSC), 2003. The 2003 NEHRP recommended provisions for new buildings and other structures, part I (provisions) and part II (commentary), FEMA 368/369, Washington, D.C.

Caliński, T., and J. Harabasz. 1974. A dendrite method for cluster analysis. *Communications in Statistics-theory and Methods* 3 (1): 1–27. doi: 10.1080/03610927408827101.

Fukushima, Y., L. F. Bonilla, O. Scotti, and J. Douglas. 2007. Site classification using horizontal-to-vertical response spectral ratios and its impact when deriving empirical ground-motion prediction equations. *Journal of Earthquake Engineering* 11 (5): 712–24. doi: 10.1080/13632460701457116.

Ghasemi, H., M. Zare, Y. Fukushima, and F. Sinaeian. 2009. Applying empirical methods in site classification, using response spectral ratio (H/V): A case study on Iranian strong motion network (ISMN). *Soil Dynamics and Earthquake Engineering* 29 (1): 121–32. doi: 10.1016/j.soildyn.2008.01.007.

Ji, K., R. Wen, Y. Ren, and Y. P. Dhakal. 2020. Nonlinear seismic site response classification using K-means clustering algorithm: case study of the September 6, 2018 Mw6. 6 Hokkaido Iburi-Tobu earthquake, Japan. *Soil Dynamics and Earthquake Engineering* 128: 105907. doi: 10.1016/j.soildyn.2019.105907.

Ji, K., Y. Ren, and R. Wen. 2017. Site classification for National Strong Motion Observation Network System (NSMONS) stations in China using an empirical H/V spectral ratio method. *Journal of Asian Earth Sciences* 147: 79–94. doi: 10.1016/j.jseaes.2017.07.032.

Konno, K., and T. Ohmachi. 1998. Ground-motion characteristics estimated from spectral ratio between horizontal and vertical components of microtremor. *Bulletin of the Seismological Society of America* 88 (1): 228–41. doi: 10.1785/BSSA0880010228.

Kotha, S. R., F. Cotton, and D. Bindi. 2018. A new approach to site classification: mixed-effects ground motion prediction equation with spectral clustering of site amplification functions. *Soil Dynamics and Earthquake Engineering* 110: 318–29. doi: 10.1016/j.soildyn.2018.01.051.

Ministry of Housing and Urban-Rural Construction of the People's Republic of China (MHURC). 2010. *Code for seismic design for buildings (GB 50011 2010)*. Beijing:China Building Industry Press. (in Chinese)

Phung, V., G. M. Atkinson, and D. T. Lau. 2006. Methodology for site classification estimation using strong ground motion data from the Chi-Chi, Taiwan, earthquake. *Earthquake Spectra* 22 (2): 511–31. doi: 10.1193/1.2198873.

Seed, H. B., M. P. Romo, J. I. Sun, A. Jaime, and J. Lysmer. 1988. The Mexico earthquake of september 19, 1985-relationships between soil conditions and earthquake ground motions. *Earthquake Spectra* 4 (4): 687–729. doi: 10.1193/1.1585498.

Specht, D. F. 1990. Probabilistic neural networks. *Neural Networks* 3 (1): 109–18. doi: 10.1016/0893-6080(90)90049-Q.

Tsai, Y. B., and M. W. Huang, 2000. Strong ground motion characteristics of the Chi-Chi, Taiwan earthquake of september 21, 1999. Institute of Geophysics, National Central University.

Wen, R., Y. Ren, Z. Zhou, and X. Li. 2014. Temporary strong-motion observation network for Wenchuan aftershocks and site classification. *Engineering Geology* 180: 130–44. doi: 10.1016/j.enggeo.2014.05.001.

Wood, H. O. 1908. Distribution of apparent intensity in San Francisco. *The California Earthquake of April* 18: 220–45.

Woolery, E. W., and R. Street. 2002. 3D near-surface soil response from H/V ambient-noise ratios. *Soil Dynamics and Earthquake Engineering* 22 (9–12): 865–76. doi: 10.1016/S0267-7261(02)00109-4.

Yaghmaei-Sabegh, S., and H. H. Tsang. 2011. A new site classification approach based on neural networks. *Soil Dynamics and Earthquake Engineering* 31 (7): 974–81. doi: 10.1016/j.soildyn.2011.03.004.

Yaghmaei-Sabegh, S., and H. H. Tsang. 2014. Site class mapping based on earthquake ground motion data recorded by regional seismographic network. *Natural Hazards* 73 (3): 2067–87. doi: 10.1007/s11069-014-1177-5.

Yaghmaei-Sabegh, S., and R. Rupakhety. 2020. A new method of seismic site classification using HVSR curves: A case study of the 12 november 2017 Mw 7.3 Ezgeleh earthquake in Iran. *Engineering Geology* 270: 105574. doi: 10.1016/j. enggeo.2020.105574.

Zhao, J. X., K. Irikura, J. Zhang, Y. Fukushima, P. G. Somerville, A. Asano, Y. Ohno, T. Oouchi, T. Takahashi, and H. Ogawa. 2006. An empirical site-classification method for strong-motion stations in Japan using H/V response ratio. *Bulletin of the Seismological Society of America* 96: 914–25. doi: 10.1785/0120050124.

Zhu, C., F. Cotton, and M. Pilz. 2020b. Detecting site resonant frequency using HVSR: fourier versus response spectrum and the first versus the highest peak frequency. *Bulletin of the Seismological Society of America* 110 (2): 427–40. doi: 10.1785/0120190186.

Zhu, C., G. Weatherill, F. Cotton, M. Pilz, D. Y. Kwak, and H. Kawase, 2020a. An open-source site database of strong-motion stations in Japan: K-NET and KiK-net. V. 1.0.0. GFZ Data Services. doi: 10.5880/GFZ.2.1.2020.006

Zhu, C., G. Weatherill, F. Cotton, M. Pilz, D. Y. Kwak, and H. Kawase. 2021. An open-source site database of strong-motion stations in Japan: K-NET and KiK-net (v1.0.0). *Soil Dynamics and Earthquake Engineering* 37 (3): 2126–49.

Zhu, C., M. Pilz, and F. Cotton. 2020c. Evaluation of a novel application of earthquake HVSR in site-specific amplification estimation. *Soil Dynamics and Earthquake Engineering* 139: 106301. doi: 10.1016/j.soildyn.2020.106301.

Appendix

Table A1. The GRNN site classification results for stations of NSMONS of China.

Station name	P1	P2	P3	Site class	Station name	P1	P2	P3	Site class	Station name	P1	P2	P3	Site class
012DAT	0.000	0.000	1.000	III	051PZT	0.000	1.000	0.000	II	053YML	0.000	1.000	0.000	II
012DZZ	0.000	0.000	1.000	III	051QCS	0.007	0.993	0.000	II	053YPC	0.000	0.000	1.000	III
012FTZ	0.000	0.001	0.999	III	051SFB	0.000	1.000	0.000	II	053YRH	0.000	0.000	1.000	III
012XAZ	0.000	0.002	0.998	III	051SWH	0.000	1.000	0.000	II	053YSX	0.000	0.000	1.000	III
012ZHB	0.000	0.000	1.000	III	051TQL	0.000	1.000	0.000	II	053ZJA	0.000	1.000	0.000	II
013DXZ	0.000	0.000	1.000	III	051WCW	0.825	0.175	0.000	I	053ZTT	1.000	0.000	0.000	I
013JZG	0.000	0.000	1.000	III	051YAD	0.194	0.806	0.000	II	062MXT	0.000	1.000	0.000	II
013ZHX	0.000	0.000	1.000	III	051YAL	0.000	1.000	0.000	II	062TCH	0.000	1.000	0.000	II
014QXU	0.000	1.000	0.000	II	051YBH	0.000	0.000	1.000	III	062YXB	0.000	0.000	1.000	III
015BYM	0.000	0.999	0.001	II	051YYL	1.000	0.000	0.000	I	062ZNI	0.000	1.000	0.000	II
015TLT	0.000	0.000	1.000	III	053BBJ	0.000	0.000	1.000	III	063DCD	0.000	1.000	0.000	II
015WLH	0.000	1.000	0.000	II	053BSL	0.000	0.000	1.000	III	064BFN	0.000	0.011	0.989	III
021NQT	0.000	1.000	0.000	II	053BWY	0.000	1.000	0.000	II	064GJZ	0.000	0.000	1.000	III
051AXY	1.000	0.000	0.000	I	053CNX	0.000	0.000	1.000	III	064JSN	0.000	0.000	1.000	III
051BCB	1.000	0.000	0.000	I	053DFY	0.000	0.000	1.000	III	064WUZ	0.000	1.000	0.000	II
051BCQ	1.000	0.000	0.000	I	053DHD	0.000	0.000	1.000	III	064YCH	0.000	0.000	1.000	III
051BTT	0.000	1.000	0.000	II	053DJL	0.000	1.000	0.000	II	065ALL	0.000	0.000	1.000	III
051BXY	1.000	0.000	0.000	I	053DSL	0.000	1.000	0.000	II	065ATS	0.999	0.001	0.000	I
051BXZ	0.000	1.000	0.000	II	053DTD	0.718	0.250	0.032	I	065BAC	0.000	1.000	0.000	II
051DJH	0.000	1.000	0.000	II	053DZF	0.000	0.935	0.065	II	065BKS	0.000	1.000	0.000	II
051EMS	0.000	1.000	0.000	II	053ENJ	0.000	0.000	1.000	III	065CYZ	0.000	1.000	0.000	II
051GXT	0.000	1.000	0.000	II	053HTJ	0.000	0.000	1.000	III	065DAQ	0.000	1.000	0.000	II
051GYZ	0.000	1.000	0.000	II	053HYC	0.634	0.000	0.366	I	065EBT	0.000	1.000	0.000	II
051HDQ	0.000	1.000	0.000	II	053JCZ	0.000	0.000	1.000	III	065EJT	0.000	1.000	0.000	II
051HDX	0.000	1.000	0.000	II	053JPW	0.000	0.000	1.000	III	065FCH	0.000	0.000	1.000	III
051HSD	1.000	0.000	0.000	I	053JZX	0.000	1.000	0.000	II	065GDL	0.000	1.000	0.000	II
051HSS	0.000	1.000	0.000	II	053LDC	0.000	1.000	0.000	II	065GLK	0.000	1.000	0.000	II
051HYY	0.001	0.999	0.000	II	053LDS	0.000	1.000	0.000	II	065HLJ	0.000	1.000	0.000	II
051JGS	0.000	1.000	0.000	II	053LDT	0.000	0.000	1.000	III	065HZW	0.000	0.000	1.000	III
051JLT	0.048	0.952	0.000	II	053LDX	0.000	0.000	1.000	III	065JIG	0.000	1.000	0.000	II
051JYC	0.000	1.000	0.000	II	053LFB	1.000	0.000	0.000	I	065JZC	0.000	1.000	0.000	II
051JYH	0.245	0.755	0.000	II	053LJH	0.000	0.000	1.000	III	065KCX	0.000	0.000	1.000	III
051JYW	0.000	1.000	0.000	II	053LLT	0.000	1.000	0.000	II	065KEL	0.856	0.000	0.144	I
051JYZ	0.000	1.000	0.000	II	053LLX	0.000	1.000	0.000	II	065KSU	1.000	0.000	0.000	I
051JZG	0.000	1.000	0.000	II	053LZH	0.002	0.998	0.000	II	065KZR	0.000	1.000	0.000	II
051JZW	1.000	0.000	0.000	I	053MMM	0.000	1.000	0.000	II	065MUS	1.000	0.000	0.000	I
051LDJ	1.000	0.000	0.000	I	053MST/ 053QJX	0.000	1.000	0.000	II	065SCH	0.000	1.000	0.000	II
051LDL	0.000	1.000	0.000	II	053NBD	1.000	0.000	0.000	I	065SLM	0.000	1.000	0.000	II
051LDS	0.000	1.000	0.000	II	053NRM	0.678	0.322	0.000	I	065SRT	0.000	0.000	1.000	III
051LSJ	1.000	0.000	0.000	I	053NRT	0.000	1.000	0.000	II	065SUF	0.000	1.000	0.000	II
051LSL	0.000	1.000	0.000	II	053PDH	0.000	1.000	0.000	II	065SYA	0.000	0.989	0.011	II
051LXK	0.000	1.000	0.000	II	053PMX	1.000	0.000	0.000	I	065TSD	0.000	1.000	0.000	II
051LXM	0.000	1.000	0.000	II	053PRX	0.001	0.000	0.999	III	065WLG	0.000	1.000	0.000	II
051LXS	0.000	1.000	0.000	II	053QCT/ 053QQC	0.000	1.000	0.000	II	065WMK	1.000	0.000	0.000	I
051MBQ	1.000	0.000	0.000	I	053QWZ	0.000	0.000	1.000	III	065WPR	1.000	0.000	0.000	I
051MCL	0.000	1.000	0.000	II	053RHT	1.000	0.000	0.000	I	065WQT	0.000	1.000	0.000	II
051MLN	0.000	1.000	0.000	II	053SML	0.008	0.992	0.000	II	065WSL	1.000	0.000	0.000	I
051MXF	1.000	0.000	0.000	I	053SSM	0.000	0.000	1.000	III	065XKR	0.000	1.000	0.000	II
051MXN	1.000	0.000	0.000	I	053TPX	0.387	0.613	0.000	II	065XTL	0.000	0.000	1.000	III
051MYS	0.000	1.000	0.000	II	053WYX	0.000	1.000	0.000	II	065YAH	0.991	0.009	0.000	I
051NNH	0.000	0.000	1.000	III	053XQD	0.000	0.000	1.000	III	065YJT	0.000	0.000	1.000	III
051PJD	0.000	1.000	0.000	II	053XXZ	0.203	0.797	0.000	II	065YPH	0.000	0.000	1.000	III
051PWD	0.000	1.000	0.000	II	053YBD	0.000	1.000	0.000	II	065YTK	0.996	0.000	0.004	I
051PWM	1.000	0.000	0.000	I	053YBX	0.000	0.000	1.000	III	065YYG	0.000	1.000	0.000	II
051PWN	0.000	1.000	0.000	II	053YCH	0.000	0.000	1.000	III	065ZYC	0.000	0.000	1.000	III
051PWP	0.979	0.021	0.000	I	053YJG	0.000	0.000	1.000	III					

Table A2. The site classification results for part of stations of NSMONS in China according to the borehole information.

Station name	V_{se}(m/s)	H^*(m)	Site class	Station name	V_{se}(m/s)	H^*(m)	Site class	Station name	V_{se}(m/s)	H^*(m)	Site class
012DAT	134	>80	II	051JZW	391	16	II	053DHD	181	>30	II
012DZZ	151	>50	II	051LDJ	265	20	II	053DJL	245	9.6	II
012FTZ	158	>80	II	051LDL	281	>20	II	053DSL	327	8.7	II
012XAZ	154	>50	II	051LDS	340	20.3	II	053JZX	336	25	II
012ZHB	159	>50	II	051LSL	213	6.4	II	053LDS	170	18.6	II
013JZG	144	30	II	051LXK	261	20	II	053LDC	170	18.6	II
014QXU	183	>50	II	051LXS	272	22	II	053LLX	250	>18	II
015BYM	354	>46	II	051LXT	230	12.6	II	053MMM	301	25	II
015TLT	238	50	II	051MCL	227	11	II	053MST/053QJX	230	18	II
015WLH	328	13	II	051MLN	259	22.3	II	053PDH	273	13	II
051AXY	340	22	II	051MXB	277	22.3	II	053RHT	Rock	–	I
051BTT	235	22	II	051MXD	Rock	–	I	053YBD	269	17.8	II
051BXZ	220	7.1	II	051MYS	300	22	II	053ZJA	223	14	II
051DJH	245	9	II	051NNH	241	>20	II	062MXT	241	20	II
051EMS	277	4.2	I	051PJD	318	>20	I	062TCH	226	14	II
051GYZ	188	11.3	II	051PWN	227	30	II	062ZNI	168	10	II
051HDQ	245	10.8	II	051PWP	394	22	II	063DCD	239	30	II
051HDX	218	12	II	051PZT	306	15	II	064BFN	180	>30	II
051HSS	324	20	II	051SFB	232	12	II	064GJZ	189	>30	II
051HYY	386	7.6	II	051SWH	186	4.1	II	064JSN	190	>30	II
051JLT	198	12	II	051TQL	281	7.8	II	064WUZ	204	26	II
051JYC	355	5.7	II	051WCW	295	15.88	II	064YCH	203	>30	II
051JYH	237	17.5	II	051YAD	190	18.5	II	065WSL	Rock	–	I
051YBH	311	14	II	051YBH	226	8.3	II				
051JZG	271	22	II	053BSL	200	>35	II				

"Rock", means that the site is classified as 'rock' according to the geology survey report.
"/", means that the station code changed.